Available online at www.sciencedirect.com
SCIENCE DIRECT®
Journal of Magnetic Resonance 167 (2004) 242–252
JMR Journal of Magnetic Resonance
www.elsevier.com/locate/jmr

Local structure in perovskite relaxor ferroelectrics: high-resolution ^{93}Nb 3QMAS NMR

Donghua H. Zhou,[a] Gina L. Hoatson,[a,*] and Robert L. Vold[b,*]

[a] *Department of Physics, College of William and Mary, P.O. Box 8795, Williamsburg, VA 23187-8795, USA*
[b] *Department of Applied Science, College of William and Mary, P.O. Box 8795, Williamsburg, VA 23187-8795, USA*

Received 16 December 2003

Abstract

Solid solutions of $(1-x)Pb(Mg_{1/3}Nb_{2/3})O_3 xPb(Sc_{1/2}Nb_{1/2})O_3$ (PMN/PSN) have been investigated using high-resolution ^{93}Nb 3-quantum magic-angle spinning nuclear magnetic resonance experiments (3QMAS NMR). In previous MAS NMR investigations, the local B-cation ordering in these relaxor ferroelectric solid solutions was quantitatively determined. However, in conventional one-dimensional MAS spectra the effects of chemical shifts and quadrupole interaction are convoluted; this, in addition to the insufficient resolution, precludes reliable extraction of the values of isotropic chemical shift and quadrupole coupling product. In the current 3QMAS investigation, ^{93}Nb spectra are presented for concentrations $x = 0$, 0.1, 0.2, 0.6, 0.7, and 0.9 at high magnetic field (19.6 T) and fast sample spinning speed (35.7 kHz). Seven narrow peaks and two broad components are observed. The unique high-resolution of the two-dimensional 3QMAS spectra enables unambiguous and consistent assignments of spectral intensities to the specific 28 nearest B-site neighbor (nBn) configurations, (N_{Mg}, N_{Sc}, N_{Nb}) where each number ranges from 0 to 6 and their sum is 6. It is now possible to isolate the isotropic chemical shift and quadrupole coupling product and separately determine their values for most of the 28 nBn configurations. The isotropic chemical shift depends linearly on the number of Mg^{2+} cations in the configuration; $\delta_{iso}^{CS} = (13.7 \pm 0.1)N_{Mg} - 970 \pm 0.4$ ppm, regardless of the ratio N_{Sc}/N_{Nb}. For the seven Nb^{5+}-deficient configurations $(N_{Mg}, 6\text{-}N_{Mg}, 0)$ and the pure niobium configuration $(0, 0, 6)$, the quadrupole coupling products (and hence the electric field gradients) are small ($P_Q \sim 6$–12 MHz) and for the remaining configurations containing small, ferroelectric active Nb^{5+} ions, the quadrupole coupling products are significantly larger ($P_Q \sim 40$ MHz), indicating larger electric field gradients.

Keywords: Multiple quantum MAS; Ferroelectric

1. Introduction

Due to their large dielectric and electromechanical effects, the relaxor ferroelectrics have important applications in capacitors, sensors, actuators, and transducers [1,2]. Most relaxors have ABO_3 pseudo-perovskite structure. Lead-based (A = Pb) solid solutions $(1-x)Pb(Mg_{1/3}Nb_{2/3})O_3 xPb(Sc_{1/2}Nb_{1/2})O_3$ (PMN/PSN) are very good systems to study these technically important relaxors, where despite years of intensive study the microscopic origin of their macroscopic behavior is still not fully understood [3,4]. The two end-members of the series, PMN and PSN, represent two types of perovskites with 1:2 and 1:1 B-cation stoichiometries, respectively. The local structure of most lead-based relaxor ferroelectrics is very different from their average crystallographic structure [5,6]. Moreover, short-range chemical disorder on either A or B cation sites seems essential for relaxor behavior i.e., the diffuse and dispersive ferroelectric to paraelectric phase transition [4]. In PSN-type perovskites, for example $PbSc_{1/2}Ta_{1/2}O_3$ (PST), the 1:1 long-range chemical order of B sites in the [1 1 1] direction needs to be frustrated for relaxor behavior to occur. Annealed PST, which has long-range chemical order, is a normal ferroelectric; while disordered PST, where there is only short-range chemical order, is a relaxor ferroelectric [7]. On the other hand for PMN-type perovskites (for example, the solid solution

* Corresponding authors. Fax: 1-7572213540 (R.L. Vold).
E-mail addresses: gina@nmr.physics.wm.edu (G.L. Hoatson), rlv@nmr.physics.wm.edu (R.L. Vold).

1090-7807/$ - see front matter © 2004 Elsevier Inc. All rights reserved.
doi:10.1016/j.jmr.2003.12.015

of $Pb(Mg_{1/3}Ta_{2/3})O_3$ and 5 mol% $PbZrO_3$) materials with and without long-range $[1\,1\,1]_{1:1}$ order can be relaxors [8]. The long-range $[1\,1\,1]_{1:1}$ ordered PMN-type ceramics are relaxor instead of normal ferroelectrics because they possess another type of disorder. According to the random site model (RS), different B-ions β' and β'' alternately occupy B-sites along the [1 1 1] direction. The β'' sites are thought to be the small ferroelectrically active Ta^{5+} cations, while the β' sites are randomly occupied by Mg^{2+}, Zr^{4+}, and the remaining Ta^{5+} cations; this results in the β' disorder [8,9].

We have studied B-site ordering quantitatively in the PMN/PSN system using ^{93}Nb magic-angle spinning (MAS) solid-state nuclear magnetic resonance (NMR) and Monte Carlo simulation [10]. For high PSN concentrations ($x > 0.5$), we showed that the random site model fits the NMR MAS data very well. However, small deviations were found at low PSN concentrations x. Quantitative agreement was obtained by modifying the RS model to include unlike-pair energies among different B-cations. As a result, cations on β' sites are no longer distributed randomly and there is the possibility of cation segregation or aggregation on the β' sublattice [10].

For PMN/PSN solid solutions the MAS spectra consist of seven narrow and two broad NMR peaks [10]. The narrow peaks are assigned to ^{93}Nb configurations with only the larger cations (Mg^{2+} and/or Sc^{3+}) occupying the six nearest B neighbor sites (nBn); and they are designated 0 through 6 according to the number of Mg^{2+} cations in the nBn configurations. The two broad peaks D_1 and D_2 were assigned to 18 and 3 nBn configurations containing Nb^{5+}, respectively. Local structural information (electron densities, wavefunctions, and electric field gradients) of these configurations is encoded in the NMR parameters; the isotropic chemical shift δ_{iso}^{CS} and quadrupole coupling product $P_Q = C_Q(1+\eta^2/3)^{1/2}$, where C_Q and η are the quadrupole coupling constant and asymmetric parameter of the electric field gradient tensor at the nuclear site. The seven narrow peaks have consistent and relatively small quadrupole coupling products ($P_Q \sim 12$ MHz) and an isotropic chemical shift, which increases by 14 ppm when a Mg^{2+} replaces a Sc^{3+} in the nBn configuration. Each of the broad peaks consists of distributions of δ_{iso}^{CS} and P_Q resulting from contributions from a variety of nBn configurations [10]. Because of spectral broadening and overlap in one-dimensional MAS spectra, it was very difficult to unambiguously and uniquely determine these two distribution functions independently. Therefore, we chose a set of distribution parameters that consistently fit PMN lineshapes collected at two magnetic fields (14 and 19.6 T), and then all the subsequent fits were constrained to use the same parameter set for all PSN concentrations. This does not affect the accuracy for the narrow peak intensities; but it may not appropriately partition the distribution intensities in D_1 and D_2. Thus, the reported results of B-site ordering [10] are valid, but the structural information derived for D_1 and D_2 using this over-simplified approach is prone to systematic errors and is intrinsically less accurate.

The main focus of the present work is to extract more accurate and precise local structural information using high-resolution two-dimensional multi-quantum MAS (MQMAS) NMR. This provides higher resolution than conventional MAS because the anisotropy in the indirect dimension is removed by eliminating the phase contribution due to the fourth rank term in the second order quadrupolar Hamiltonian [11,12]. This is accomplished through correlation of the 3-quantum coherence $(3/2 \leftrightarrow -3/2)$ in the evolution period with single-coherence $(1/2 \leftrightarrow -1/2)$ in the detection period; meanwhile MAS eliminates the second rank term. With the additional isotropic dimension, both isotropic chemical shift and quadrupole coupling product can be determined from a 3QMAS experiment at a single magnetic field. Consequently, a distribution of chemical shifts can be disentangled from a distribution of quadrupole coupling products.

2. Experimental methods

The $(1-x)$ PMN/PSN solid solutions are the same materials as used for MAS [10] and were kindly provided by Dr. Peter Davies (University of Pennsylvania). They are well-characterized by X-ray diffraction (XRD), transmission electron microscopy (TEM), and dielectric measurements [13]. 3QMAS NMR experiments were performed on samples with concentrations $x = 0$, 0.1, 0.2, 0.6, 0.7, and 0.9; all except the PMN ($x = 0$) were thermally treated, well-ordered materials.

Because of fast T_1 (<50 ms) and T_2 (<0.5 ms) relaxation times, the three-pulse Z-filter 3QMAS sequence [14] was used to collect hypercomplex data at 19.6 T ^{93}Nb resonance frequency $\nu_L = 203.05$ MHz. The optimized pulse widths were 2.5, 0.7, and 5 μs, respectively. The RF field strength was 75 kHz for the first two pulses, and 10 kHz for the third (selective) pulse. The interval between the second and third pulses was synchronized to one rotor period, 28 μs (rotor of diameter 2 mm was spinning at 35.7 kHz); 512 complex data points were collected with dwell time 14 μs in the direct acquisition dimension; 32 time increments $\Delta t_1 = 28$ μs were used in the indirect acquisition dimension; and 4000 scans were accumulated with 100 ms relaxation delay. A solution of $NbCl_5$ in acetonitrile was used as the chemical shift reference.

Spectra were processed using customized NMRPIPE [15] following the steps (including the shear transformation) described by Massiot et al. [16]. Gaussian

broadening of width 100 Hz was applied to the direct (or MAS) dimension following the echo centers; but no apodization was applied to the indirect (isotropic) dimension. In the resulting 3QMAS spectrum of a spin $I = 9/2$ nucleus, the frequency in the isotropic dimension is given by [16]:

$$\delta_{\mathrm{id}} = \frac{17}{127}\delta_{\mathrm{iso}}^{\mathrm{CS}} - \frac{10}{27}\delta_{\mathrm{iso}}^{\mathrm{2Q}} \tag{1}$$

and the frequency in the MAS dimension is

$$\delta_{\mathrm{MAS}} = \delta_{\mathrm{iso}}^{\mathrm{CS}} + \delta_{\mathrm{iso}}^{\mathrm{2Q}} + \delta_{\mathrm{aniso}}^{\mathrm{2Q}}, \tag{2}$$

where

$$\delta_{\mathrm{iso}}^{\mathrm{2Q}} = -AP_{\mathrm{Q}}^2, \quad \delta_{\mathrm{aniso}}^{\mathrm{2Q}} = AP_{\mathrm{Q}}^2 F(\theta,\phi,\eta) \tag{3}$$

with constant A given by

$$A \equiv \frac{3x10^5[I(I+1) - 3/4]}{[2I(2I-1)]^2 \nu_{\mathrm{L}}^2} \tag{4}$$

for ^{93}Nb at 19.6 T, $A = 0.0337$ ppm/MHz^2. The angles (Θ, ϕ) define the crystallite orientation, and

$$\begin{aligned} F(\theta,\phi,\eta) = \frac{1}{96+3\eta^2}[&-54 - 3\eta^2 + 60\eta\cos 2\phi \\ &- 35\eta^2\cos 4\phi + (540 + 30\eta^2 \\ &- 480\eta\cos 2\phi + 70\eta^2\cos 4\phi)\cos^2\theta \\ &- (630 + 35\eta^2 - 420\eta\cos 2\phi + 35\eta^2 \\ &\times \cos 4\phi)\cos^4\theta] \end{aligned} \tag{5}$$

is an orientation dependent function, which averages to zero and is responsible for the second order quadrupolar powder pattern lineshape. The quadrupolar product is $P_{\mathrm{Q}} = C_{\mathrm{Q}}(1+\eta^2/3)^{1/2}$, where the quadrupolar coupling constant is defined as $C_{\mathrm{Q}} = e^2 q_{ZZ} Q/\hbar$, where $\hbar$ is Planck's constant, e is the electron charge (magnitude), q_{ZZ} is the largest principal component of the electric field gradient (EFG) tensor, and $\eta = (q_{XX} - q_{YY})/q_{ZZ}$ is the asymmetry parameter. In the MAS dimension, the "center of mass" (barycenter) of the lineshape is determined by

$$\langle \delta_{\mathrm{MAS}} \rangle = \delta_{\mathrm{iso}}^{\mathrm{CS}} + \delta_{\mathrm{iso}}^{\mathrm{2Q}}, \tag{6}$$

where $\langle\rangle$ means averaging over all crystallite orientations in the powder samples.

3. Results

^{93}Nb 3QMAS spectra for six concentrations of the solid solutions $(1-x)$PMN/xPSN are presented in Fig. 1.

In the Fig. 1, line A and a set of parallel lines B_i $(i = 0, 1, \ldots, 6)$ are convenient for discussion and can be deduced from Eq. (1)–(3) as follows. Line A, the chemical shift (distribution) axis, has slope 17/127 and it passes through points corresponding to $P_{\mathrm{Q}} = 0$. The equation for this line is

$$\delta_{\mathrm{id}} = (17/127)\delta_{\mathrm{MAS}}. \tag{7}$$

Sites with equal quadrupole product but different isotropic chemical shift appear parallel to this line. Moreover, the "center of mass" of every site is constrained to be below line A. The lines B_i are the isotropic quadrupole (distribution) axes and have slope −10/127; the equation for a B-line is

$$\delta_{\mathrm{id}} = -\frac{10}{127}\delta_{\mathrm{MAS}} + \frac{27}{127}\delta_{\mathrm{iso}}^{\mathrm{CS}}, \tag{8}$$

where $\delta_{\mathrm{iso}}^{\mathrm{CS}}$ is a fixed value. Sites with equal $\delta_{\mathrm{iso}}^{\mathrm{CS}}$ but different P_{Q} appear parallel to these lines. The seven B_i lines pass through the positions of the seven narrow peaks in spectra. For crystalline materials with well-defined crystal sites, the lineshape contours of each site should be parallel to the MAS dimension. However, in amorphous materials or in crystalline materials (such as the relaxor ferroelectrics) where many different cations can occupy crystallographically equivalent sites, there could be quasi-continuous distributions of NMR parameters. Any distribution of parameters results in contours that are slanted instead of parallel to the MAS dimension [17,18]. Because of high correlation between the fitting parameters, the axes of distribution (A and B_i) are central to the extraction of unique and unambiguous values $\delta_{\mathrm{iso}}^{\mathrm{CS}}$, P_{Q}, and populations for the distributions D_1 and D_2. Without this knowledge no meaningful interpretation of the changes of values $\delta_{\mathrm{iso}}^{\mathrm{CS}}$ and P_{Q} would be possible.

To reiterate the critical role of the distribution axes in interpreting the NMR parameters, consider an example. In Fig. 2 we try to fit the lineshape of a slice taken from the PMN 3QMAS spectrum, Fig. 1A at $\delta_{\mathrm{id}} = -120$ ppm. The slice appears to be an overlap of two peaks; for each peak, there are numerous pairs of $\delta_{\mathrm{iso}}^{\mathrm{CS}}$ and P_{Q} values which give acceptable fits to the lineshape, with appropriate amounts of line broadening. Two equally good fits with rather different parameters are presented in Figs. 2A and B. In Fig. 2A, the narrow peak is fit with parameters $\delta_{\mathrm{iso}}^{\mathrm{CS}} = -891.5$ ppm, $P_{\mathrm{Q}} = 10$ MHz, and lorentzian broadening of 3.5 ppm; the broad peak is fit with $\delta_{\mathrm{iso}}^{\mathrm{CS}} = -911$ ppm, $P_{\mathrm{Q}} = 31$ MHz, and lorentzian broadening of 6 ppm. In Fig. 2B, the narrow peak is fit with $\delta_{\mathrm{iso}}^{\mathrm{CS}} = -894.5$ ppm, $P_{\mathrm{Q}} = 5$ MHz, and lorentzian broadening of 7 ppm; the broad peak is fit with $\delta_{\mathrm{iso}}^{\mathrm{CS}} = -930$ ppm, $P_{\mathrm{Q}} = 20$ MHz, and lorentzian broadening of 18 ppm. The failure of this slice-fitting approach to yield unique parameters, which is routinely used to extract NMR parameters from 3QMAS spectra of crystalline materials [12] is due to the absence of characteristic lineshape features. This is caused by disorder in the relaxor ferroelectrics. (For a simple second order quadrupolar lineshape, there are usually two peaks and several discontinuities, which sensitively depend on the value of η.)

In our previous ^{93}Nb MAS NMR study, components of ^{93}Nb MAS spectra were assigned according to con-

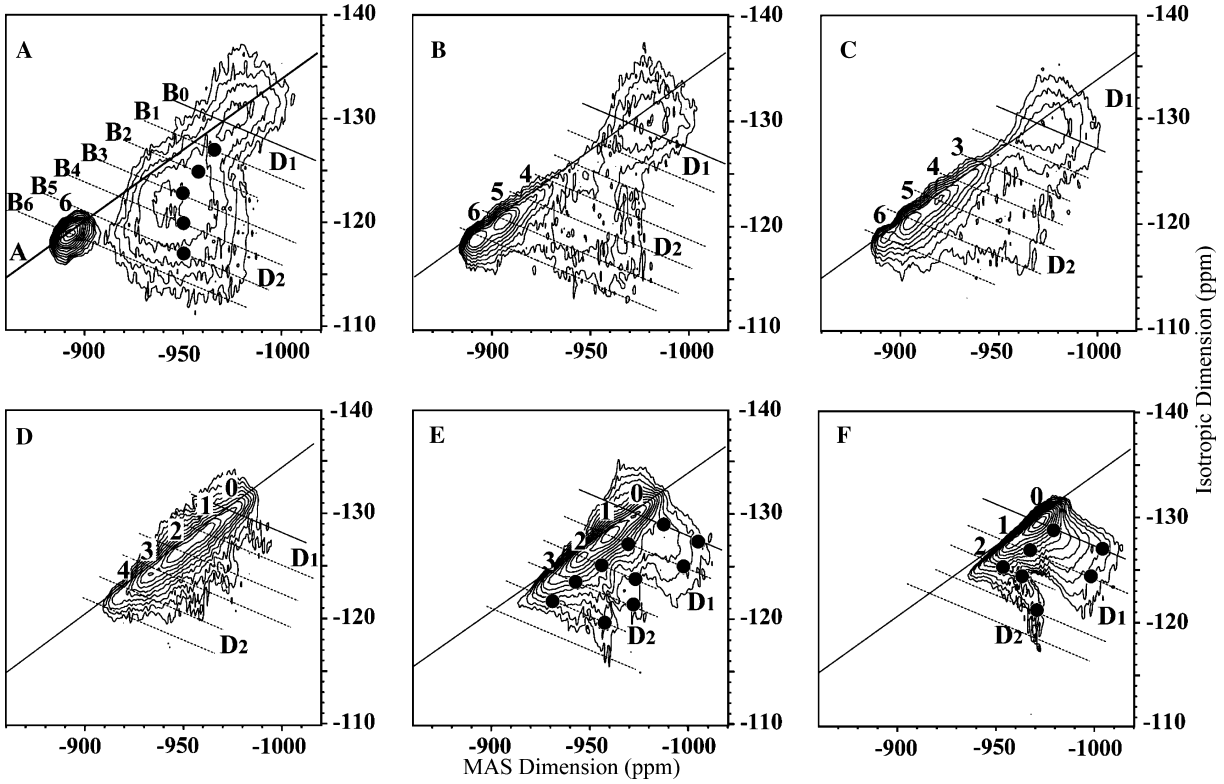

Fig. 1. ^{93}Nb 3QMAS spectra for $(1-x)$PMN/xPSN solid solutions, with concentrations $x = 0$ (A), 0.1 (B), 0.2 (C), 0.6 (D), 0.7 (E), and 0.9 (F). Line A has slope 17/127; lines B_i $(i = 0, 1, \ldots, 6)$ have slope −10/127 and pass through positions of narrow peaks (see text for definitions). The contour levels start from 80% and decrease by factor 0.8. Different contour numbers are chosen so as to display signals with similar noise strength; 12 levels in (A) and (E) with 6.9% minimum, 9 in (B) with 13.4% minimum, 8 in (C) with 16.8% minimum, 10 in (D) with 10.7% minimum, and 14 in (F) with 4.4% minimum. Filled circles mark the sampling points whose coordinates are used to calculate NMR parameters (see text).

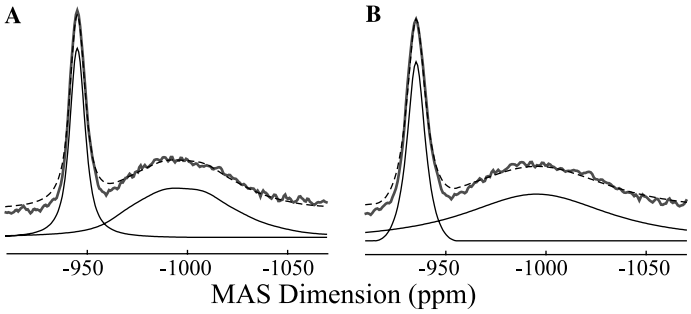

Fig. 2. Lineshape fits for a slice taken from the PMN 3QMAS spectrum Fig. 1A at $\delta_{id} = -120$ ppm. The bold solid line is the experimental spectrum, thin solid lines are fitting components, and the dashed line is the sum of the two components. Equally good fits are obtained in (A) and (B) with very different parameters given in the text.

figurations of the six nearest B-site neighbors (nBn); (N_{Mg}, N_{Sc}, N_{Nb}), where N_{Mg} is the number of Mg^{2+} ions in the nBn (with analogous definitions of N_{Sc} and N_{Nb}), so that $N_{Mg} + N_{Sc} + N_{Nb} = 6$ [10]. NMR parameters are strongly affected by nBn configurations since the three types of B-cations are different in valence, size, and electronegativity; Mg^{2+} (ionic radius 0.72 Å, Pauling scale electronegativity 1.31), Sc^{3+} (0.745 Å, 1.36), and Nb^{5+} (0.64 Å, 1.60) [19,20]. In strong contrast with Nb^{5+} cations, Mg^{2+} and Sc^{3+} cations have similar size and electronegativity and a smaller charge difference. The nBn configurations with only Mg^{2+} and/or Sc^{3+} cations have closest to cubic symmetry, and thus small electric field gradients (EFGs). These Nb^{5+}-deficient configurations $(N_{Mg}, 6\text{-}N_{Mg}, 0)$, with $N_{Mg} = 6, 5, \ldots, 0$ give rise to the seven narrow peaks observed. On the other hand, charge, size, and electronegativity mismatches resulting from mixing Nb^{5+} with Mg^{2+}/Sc^{3+} severely distorts local cubic symmetry. This leads to larger EFGs, and consequently greater quadrupole

parameters and linewidths. The broad lineshapes associated with a variety of configurations containing Nb^5 cannot be resolved, and they give rise to the two broad distributions D_1 and D_2.

3.1. PMN

The PMN 3QMAS spectrum (Fig. 1A) reveals three sites; one narrow peak corresponding to ^{93}Nb with six Mg^{2+} nearest B neighbors (label 6) and two broad distribution peaks labeled D_1 and D_2, respectively. One may compare their quadrupole products P_Q instantly by their distances from chemical shift axis (line A). The "mass centers" of peaks 6 and D_1 are very close to line A, therefore these peaks have small and similar P_Qs. The center of peak D_2 is far from line A and thus a much larger P_Q is expected. The NMR parameters δ_{iso}^{CS} and P_Q may be estimated from the coordinates of "mass centers" $(\langle\delta_{MAS}\rangle, \delta_{id})$ by solving Eqs. (1) and (6). These coordinates are best determined by varying contour spacing until a very small closed contour is seen around a peak; spacing with a factor of 0.95 usually works. The results are summarized in Table 1.

For peak 6, the quadrupole product 9.0 MHz agrees with the value 8.9 MHz found in another 3QMAS study by Cruz et al. [21], but is somewhat smaller than the 12 MHz value estimated in our previous analysis of the spinning-sideband manifold in a MAS spectrum [10]. Peak 6 has small distributions of NMR parameters and these may be caused by effects of cations further away than the nearest B cations, or by residual dipolar coupling. The evidence for distributions of δ_{iso}^{CS} and P_Q is that the contours of this peak (Fig. 1A) are not parallel to the MAS dimension. For example, a point with coordinates (−892.6, −118.4) ppm, which is only 0.5 ppm away from the "mass center," gives $P_Q = 12.3$ MHz and $\delta_{iso}^{CS} = -887.5$ ppm.

In the 3QMAS spectrum for PMN obtained by Cruz et al. (at 9.4 T with rotor speed 14 kHz), only one broad peak is identified, with $P_Q = 21.5$ MHz [21]. This is closest to the broad peak D_2 in our spectrum, for which $P_Q = 27.3$ MHz is obtained from the "mass center" of the peak. The high magnetic field strength (19.6 T) and fast sample spinning speed (35.7 kHz) used in our 3QMAS experiment help to unambiguously resolve the other broad peak. This additional peak, D_1, has $P_Q = 9.4$ MHz and $\delta_{iso}^{CS} = -973$ ppm.

Large distributions of NMR parameters are evident for peaks D_1 and D_2 since the lineshapes are very broad and featureless. In PMN, there are seven nBn configurations; $(N_{Mg}, 0\text{-}N_{Mg}, 6)$, with $N_{Mg} = 1, 2, \ldots, 6$. In Section 3.2 we will show that the isotropic chemical shift of any nBn configuration (N_{Mg}, N_{Sc}, N_{Nb}), is mainly determined by the number of Mg^{2+} cations and is independent of the ratio N_{Sc}/N_{Nb}. Along each of the seven quadrupole distribution axes B_i shown in Fig. 1, the δ_{iso}^{CS} value is solely determined by $N_{Mg} = i$. The quadrupole products of configurations with N_{Mg} 6 and 0 have been determined to be 9.0 and 9.4 MHz Table 1. The quadrupole products of the remaining 5 configurations may be estimated from the coordinates of the 5 sampling points (marked by filled circles in Fig. 1A); $P_Q = 38 \pm 3$, 32 ± 3, 24 ± 2, 20 ± 2, and 19 ± 2, respectively for $N_{Mg} = 5$, 4, 3, 2, and 1. The quadrupole products of the seven configurations ($N_{Sc} = 0$ refers to PMN, which has no Scandium) are plotted against the Mg^{2+} cation number in Fig. 3.

The pure-magnesium $(6, 0, 0)$ and pure-niobium $(0, 0, 6)$ configurations have small P_Q because of high symmetry. For configurations with both Mg^{2+} and Nb^{5+} the cation mismatch lowers the symmetry, and therefore larger P_Q values are reasonable. It is interesting to notice that the five Mg, one Nb configuration $(5, 0, 1)$ has the largest P_Q. The large quadrupole coupling of this configuration causes the resonance to shift in the lower-left direction along the quadrupole distribution axis B_5 in Fig. 1; this explains the gap between narrow peak 6 and the broad peak D_2 (this is also observed in the MAS spectrum of PMN) [10].

3.2. (1 − x) PMN/x PSN: narrow peaks

In the spectrum of the solid solution with $x = 0.1$ (Fig. 1B) two more narrow peaks (labeled 5 and 4) are

Table 1
NMR parameters for the narrow peak (6) and the two broad peaks D_1 and D_2 of PMN

	$(\langle\delta_{MAS}\rangle, \delta_{id})$ (ppm)	δ_{iso}^{CS} (ppm)[a]	P_Q (MHz)[b]
6	(−892.6, −118.9)	−889.9, −907[c]	9.0, 8.9[c]
D_1	(−944.0, −121.0)	−918.8, −925[c]	27.3, 21.5[c]
D_2	(−976.0, −130.0)	−973.0	9.4

[a] Errors for δ_{iso}^{CS} are ±0.5 ppm.
[b] Errors for P_Q are ±1 MHz.
[c] These values were obtained from [21], where the chemical shift was referred to solid Nb_2O_5 and has been re-calculated here to refer to our standard Nb/MeCN solution.

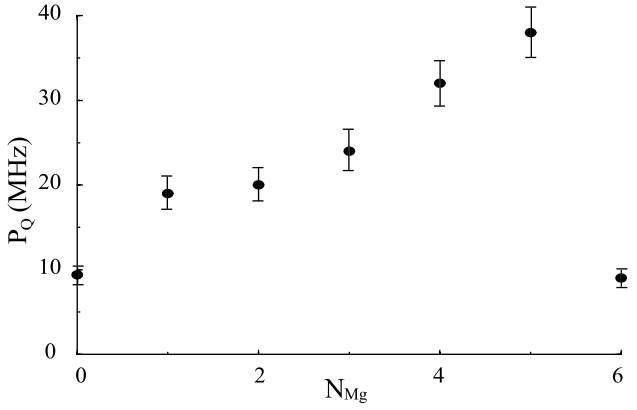

Fig. 3. ^{93}Nb quadrupole products of the seven nearest neighbor configurations in PMN/PSN containing only Mg^{2+} and Nb^{5+} cations.

observed in addition to the narrow peak 6, which is the only narrow peak observed in PMN spectrum. For $x = 0.2$ (Fig. 1C) one more narrow peak 3 is observed. For $x = 0.6$ (Fig. 1D), peak 6 disappears completely and peak 5 is very weak. Meanwhile, new narrow peaks 2, 1, and 0 are observed. For $x = 0.7$ (Fig. 1E), peak 5 disappears completely and peak 4 becomes weak. For $x = 0.9$ (Fig. 1F), narrow peak 3 also disappears. The NMR parameters δ_{iso}^{CS} and P_Q of these peaks are calculated from their coordinates in the spectra and summarized in Fig. 4.

The seven narrow peaks have been assigned to the seven Nb^{5+}-deficient configurations (N_{Mg}, 6-N_{Mg}, 0) with $N_{Mg} = 0, 1, \ldots, 6$; with this notation N_{Mg} coincides with the number used to label each peak. The isotropic chemical shift is linearly correlated with the number of Mg^{2+} cations in the nBn configuration,

$$\delta_{iso}^{CS} = 13.7(\pm 0.1)N_{Mg} - 970.0(\pm 0.4). \quad (9)$$

This means replacing each Mg^{2+} ion by a Sc^{3+} ion causes −13.7 ppm shift. An analogous linear dependence has been observed for ^{207}Pb isotropic chemical shift in mixed crystals of lead/strontium nitrate [(Pb,Sr)$(NO_3)_2$] and lead/barium nitrate [(Pb,Ba)$(NO_3)_2$] [22]. In each of the mixed crystals, 13 ^{207}Pb resonance lines were observed due to lead ions with 0–12 Pb^{2+} nearest-neighbor cations replaced by Sr^{2+} or Ba^{2+}. The observed average shift is 22 ppm per Sr^{2+} ion and 19 ppm per Ba^{2+} ion.

For the quadrupole product the data, though more scattered with concentration x, can be fit to a quadratic dependence on the number of Mg^{2+} cations

$$P_Q = -0.23(\pm 0.06)N_{Mg}^2 + 1.8(\pm 0.4)N_{Mg} + 7.2(\pm 0.5). \quad (10)$$

The fitting curve (Fig. 4B) shows that mixing of Mg^{2+} and Sc^{3+} cations in a nBn configuration slightly increases the electric field gradient at the central ^{93}Nb site, which seems intuitively reasonable.

The applicability of the empirical relationship between δ_{iso}^{CS} and N_{Mg} (Eq. (9)) deduced for the Nb^{5+}-deficient nBn configurations may be generalized to configurations which contain Nb^{5+} cations. This generalization is based on the observation that the highest contour of 0.1PMN–0.9PSN, which locates the all scandium nBn configuration [peak 0, (0, 6, 0)], almost coincides with the D_1 "mass center" of PMN, which corresponds to the all niobium configuration [(0, 0, 6)] (see Figs. 1A and F). The six-Sc and six-Nb configurations have similar NMR parameters; $P_Q = 8.4$, 9.4 MHz and $\delta_{iso}^{CS} = -969.6$, −973 ppm, respectively. The small P_Q values imply that these two configurations are both highly symmetric; ion displacements must be small or dynamically averaged. However, without detailed ab initio calculations it cannot be understood why the two configurations should have such similar δ_{iso}^{CS} values. Nevertheless, the similarity of δ_{iso}^{CS} for the (0, 6, 0) and (0, 0, 6) configurations suggests that the isotropic chemical shift of any nBn configuration (N_{Mg}, N_{Sc}, N_{Nb}) is determined primarily by N_{Mg}, while the ratio N_{Sc}/N_{Nb} only results in minor adjustment. This generalization will be prove to be very important in interpreting the NMR parameters of other nBn configurations (and in fact, it was used in Section 3.1 to interpret the configurations with only Mg^{2+} and Nb^{5+}).

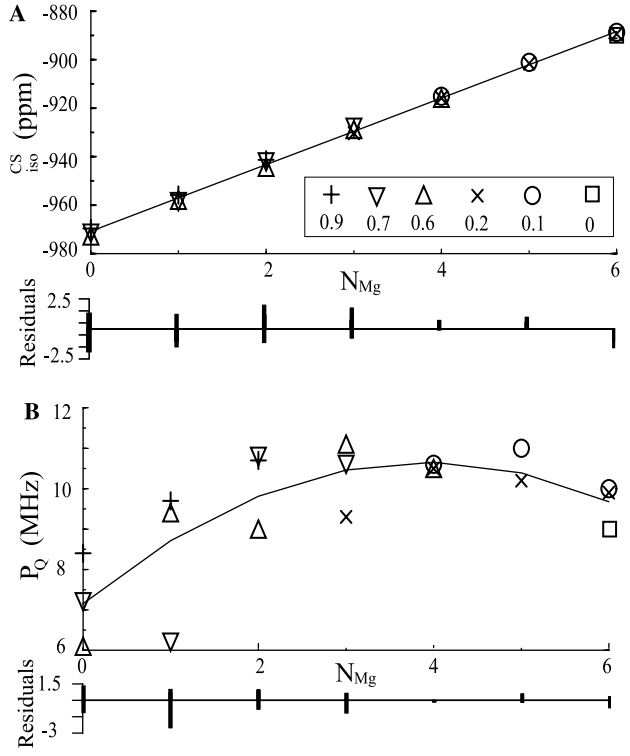

Fig. 4. Isotropic chemical shifts (A) and quadrupole products (B) of the seven narrow peaks in ^{93}Nb 3QMAS spectra of $(1-x)$PMN–xPSN. Each concentration x is marked with a unique symbol (see legend in the inset of (A)). These peaks have only Mg^{2+} and Sc^{3+} cations as their nearest B-site neighbors, (N_{Mg}, 6-N_{Mg}, 0). Linear fit in (A) gives $\delta_{iso}^{CS} = 13.7(\pm 0.1)N_{Mg} - 970.0(\pm 0.4)$ ppm with correlation coefficient $R = 0.998$. Quadratic fit in (B) gives $P_Q = -0.23(\pm 0.06)N_{Mg}^2 + 1.8(\pm 0.4)N_{Mg} + 7.2(\pm 0.5)$ MHz with $R = 0.663$. The residuals are plotted below each sub-figure.

3.3. $(1-x)$PMN/xPSN: broad distribution peaks

In PMN, the two distributions D_1 and D_2 which were severely overlapped in the one-dimensional MAS spectra [10], are clearly resolved in the high-resolution two-dimensional 3QMAS spectrum (Fig. 1A). As PSN concentration x increases from 0 to 0.1, 0.2, and 0.6 (Figs. 1B, D, and E), D_1 and D_2 intensities progressively decrease. However, at $x = 0.6$ (Fig. 1D) the D_1 intensity starts growing back but with a new shape. The new D_1 has very strong intensities in 3QMAS spectra of concentrations $x = 0.7$ and 0.9 (Figs. 1E and F). In

addition, the D_2 distribution also has a new shape in high concentrations ($x = 0.7$ and 0.9, Figs. 1E and F).

By inspection of the 3QMAS spectra of all solid solutions (Fig. 1), it can be seen that a quadrupole distribution axis positioned midway between lines B_1 and B_2 marks an appropriate boundary between the two distributions D_1 and D_2. With the assistance of the generalized relationship between isotropic chemical shift and N_{Mg} established in the preceding subsection, it is reasonable to assign D_1 to configurations (N_{Mg}, N_{Sc}, N_{Nb}) with $N_{Mg} = 0$ or 1 and $N_{Nb} \neq 0$. D_2 then includes the rest of the $N_{Nb} \neq 0$ configurations with $N_{Mg} = 2, 3, 4, 5$. These assignments are subtly different from the previous one [10] based on the MAS spectra, where D_1 was assigned to configurations with $N_{Mg} = 0, 1, 2, 3$ and $N_{Nb} \neq 0$, and D_2 to $N_{Mg} = 4$, 5 with $N_{Nb} \neq 0$. The new, unambiguous assignments proposed here should supersede the old ones [10]; the difference illustrates the uncertainty and ambiguity in deconvoluting overlapping lines in one-dimensional MAS spectra. The new assignments, together with the previous ones for comparison, are shown in Fig. 5.

Analyses of spectra for $x = 0.7$ and 0.9 (Figs. 1E and F) provide NMR parameters for more nBn configurations. Along quadrupole distribution axis B_0 (in both Figs. 1E and F), two points are sampled (marked with filled circles in the figures) to give an estimated P_Q range of 20–32 MHz for nBn configurations with $(0, N_{Sc}, 6\text{-}N_{Sc})$ and $N_{Sc} = 1, 2, \ldots, 5$. Similarly, along line B_1 in Figs. 1E and F, two points are sampled to give an estimated P_Q range of 20–37 MHz for nBn configurations with $(1, N_{Sc}, 5\text{-}N_{Sc})$ and $N_{Sc} = 0, 1, \ldots, 4$.

Along line B_2 in Fig. 1E for $x = 0.7$, the P_Q range 20–30 MHz is found for nBn configurations $(2, N_{Sc}, 4\text{-}N_{Sc})$ and $N_{Sc} = 0, 1, 2, 3$; in Fig. 1f for $x = 0.9$, the range is 20–25 MHz. Intuitively, the smaller range at concentration 0.9 is caused by the disappearance of configurations with smaller number of Sc^{3+}, while the configurations with more Sc^{3+} cations persist. According to the random site (RS) model of B cation ordering [8,9], the intensities for $(2, 0, 4)$, $(2, 1, 3)$, $(2, 2, 2)$, and $(2, 3, 1)$ are 0.0, 0.2, 1.6, and 7.5% at $x = 0.7$ and are 0.0, 0.0, 0.0, and 0.6% at $x = 0.9$, respectively [10]. The actual intensities may be slightly different from these since the RS model agrees only qualitatively with MAS NMR peak intensities. Nevertheless, trends given by the RS model agree with intuition. Thus, the configurations $(2, 0, 4)$ and $(2, 1, 3)$ have P_Q range 25–30 MHz while configurations $(2, 3, 1)$ and $(2, 2, 2)$ have P_Q ranging from 20 to 25 MHz. For $N_{Mg} = 2$ the trend appears to be that the more niobium cations in configuration, the larger the quadrupole product.

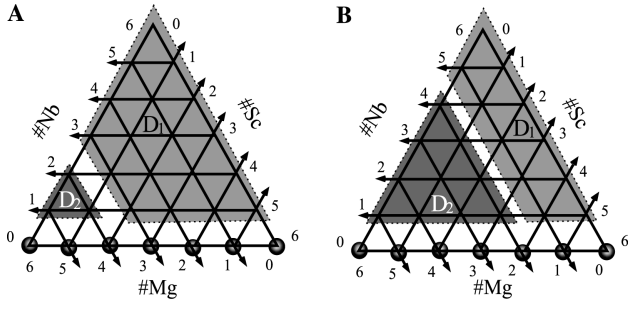

Fig. 5. The 28 nBn configurations of Nb^{5+} cations and their assignments. For a given grid point, the three vectors pointing to the axes indicate the numbers of each cation, and thus the triplet coordinate (N_{Mg}, N_{Sc}, N_{Nb}). The seven configurations on the bottom line are assigned to the narrow resonance lines. In (A) according to the previous MAS NMR study [10], the 18 configurations in the shaded trapezoid were assigned to D_1 and the three configurations in the shaded triangle were assigned to D_2. However, as shown in (B) according to the current, less ambiguous high-resolution 3QMAS results, the 11 configurations in the trapezoid belong to D_1 and the 10 configurations in the triangle are assigned to D_2.

Along line B_3 in Fig. 1E for $x = 0.7$, the P_Q range 20–35 MHz is found for configurations $(3, 0, 3)$, $(3, 1, 2)$, and $(3, 2, 1)$; in Fig. 1F for $x = 0.9$, only intensity with large $P_Q = 35$ MHz persists. Again, this intensity is assigned to the configuration with relatively more Sc^{3+} cations, $(3, 2, 1)$. For $N_{Mg} = 3$, the trend is reversed from that for $N_{Mg} = 2$; the fewer niobium cations in the configuration, the larger the P_Q. The two Sc, one Nb configuration has a larger EFG than the one Sc, two Nb configuration. According to predictions of the RS model, the respective intensities for $(3, 0, 3)$, $(3, 1, 2)$, and $(3, 2, 1)$ are 0.0, 0.3, and 2.1% at $x = 0.7$ and 0.0, 0.0, and 0.1% at $x = 0.9$ [10]; again deviations from these model predictions should be interpreted with caution.

Along line B_4 in Fig. 1E for $x = 0.7$, the P_Q range 20–35 MHz is found for nBn configurations $(4, 0, 2)$ and $(4, 1, 1)$; in Fig. 1F for $x = 0.9$, only intensity with large $P_Q = 35$ MHz persists. Again, this intensity is assigned to the Sc^{3+}-rich configuration, $(4, 1, 1)$. For $N_{Mg} = 4$, mixing one Sc and one Nb results in larger EFG than those in both the two Sc, no Nb and no Sc, two Nb configurations. The RS model predicts intensities 0.0 and 0.3% for $(4, 0, 2)$ and $(4, 1, 1)$, respectively at $x = 0.7$ and 0.0 and 0.0% at $x = 0.9$ [10]. Thus, 3QMAS intensities observed for these configurations, though very weak, reveal the small deviation of the RS model from the observed intensities.

Along line B_5 in Fig. 1E for $x = 0.7$, only a little intensity appear. $P_Q \sim 40$ MHz is found for the nBn configuration $(5, 0, 1)$, which agrees with the value 38 ± 3 MHz (Fig. 3) found by sampling a point in PMN spectrum (Fig. 1A). In Fig. 1F for $x = 0.9$, this intensity disappears. The RS model predicts results zero intensity for this configuration at both $x = 0.7$ and 0.9 [10]; this again emphasizes the high sensitivity of 3QMAS NMR and the small deviation of observed intensities from predictions of the RS model.

In summary, the assignments and NMR parameters are represented in the schematic 3QMAS spectra shown in Fig. 6.

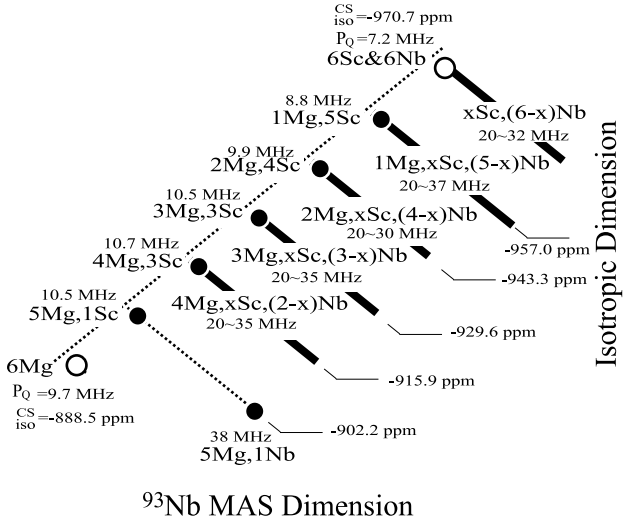

Fig. 6. Schematic 3QMAS spectra of ^{93}Nb in PMN/PSN system with assignments and NMR parameters. Empty circles denote pure nearest B-site neighbor (nBn) configurations, filled circles denote mixed configurations, and bold lines denote distributions with more than one configuration. The sum is six of three non-negative integers proceeding atoms (Mg, Sc, and Nb); $x > 0$. NMR parameters δ_{iso}^{CS} and P_Q specific to assigned nBn configurations are also shown.

The isotropic chemical shift δ_{iso}^{CS} depends only on the number of Mg and is calculated using Eq. (9). For narrow peaks (with no Nb^{5+}) the quadrupole product P_Q is calculated according to Eq. (10). P_Q values or ranges for all other nBn configurations are results given in this section. D_1 and D_2, which are newly partitioned in the beginning of this section, have the following distribution parameters. For D_1, P_Q varies between 20 and 37 MHz, and δ_{iso}^{CS} is in the range −971 to −957 ppm (from Eq. (9) with $N_{Mg} = 0, 1$); in contrast to the previous MAS partition [10] which had δ_{iso}^{CS} in the range −971 to −930 ppm with $N_{Mg} = 0, 1, 2, 3$. For D_2, P_Q is in the range 25–40 MHz, and δ_{iso}^{CS} varies between −943 and −902 ppm (Eq. (9) with $N_{Mg} = 2$–5); in contrast the previous partition [10] has δ_{iso}^{CS} range −902 to −916 ppm with $N_{Mg} = 4, 5$.

4. Discussion

This detailed 3QMAS analysis confirms the structural information from the previous MAS study for the seven narrow peaks [10]. In the nBn configurations (N_{Mg}, 6-N_{Mg}, 0), we find an empirical relationship between δ_{iso}^{CS} and N_{Mg}: increasing N_{Mg} by one causes an approximately 13.7 ppm increase in δ_{iso}^{CS} and a small variation in P_Q. This relation has been generalized for any nBn configuration (N_{Mg}, N_{Sc}, N_{Nb}), i.e., δ_{iso}^{CS} is mainly determined by N_{Mg} while N_{Sc} and N_{Nb} have only minor effects. Since the valence, ionic radii, and electronegativities of Mg^{2+} and Sc^{3+} are similar and differ markedly from those of Nb^{5+}, it is hard to understand why Sc^{3+} and Nb^{5+} have similar effects on the chemical shift of the center niobium. One possible explanation could be that Sc and Nb (but not Mg) have occupied d orbitals which may contribute to low lying excited electronic states and hence influence chemical shift.

The quadrupole products of many nBn configurations have also been extracted. It is interesting to notice that configuration (5, 0, 1) has P_Q double that of configuration (1, 0, 5); 40 versus 19 MHz. The environments of the two nBn configurations are shown in Fig. 7.

The distortion of the O_6 octahedron, which is the immediate surrounding of the center niobium, has the greatest influence on the electric field gradients. According to Chen et al. [24] the larger Mg^{2+} cation pushes the oxygen ion toward the smaller Nb^{5+} cation in the

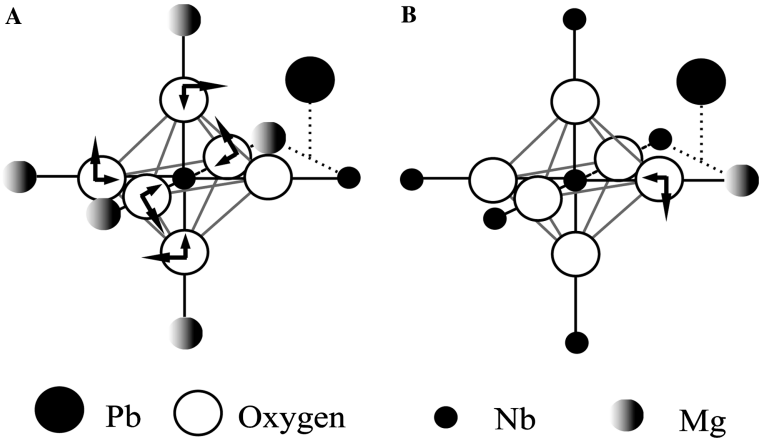

Fig. 7. The two Sc-deficient nearest B-site (nBn) configurations: (A) (5,0,1) with five Mg, one Nb and (B) (1,0,5) with one Mg, five Nb. The larger Mg^{2+} cation pushes oxygen ion toward the smaller cation Nb^{5+} in the center; moreover, the size mismatch of the ions results in transverse displacement of the oxygen ions. According to Bonneau et al. [23] the longitudinal displacement is 0.07 Å and the transverse displacement is 0.13 Å. The more distorted O_6 octahedron in (A) results in larger electric field gradients than in (B).

center. Moreover, size mismatch, which here means the sum of ionic radii $r_{Mg^{2+}} + 2r_{O^{2-}} + r_{Nb^{5+}} = 4.16\,\text{Å}$ is greater than the unit cell parameter $a = 4.05\,\text{Å}$ for PMN, results in transverse displacement of the oxygen ions [6]. According to the results of the powder neutron diffraction refinements of PMN at 307 °C [23], the longitudinal displacement is 0.07 Å and the transverse displacement is 0.13 Å. These result in a larger O_6 distortion in the $(5,0,1)$ configuration than in the $(1,0,5)$ configuration (Fig. 7). This effect may account for the larger electric field gradient and quadrupole product of the $(5,0,1)$ configuration.

We have identified most of the underlying sites and calculated their NMR parameters from the ^{93}Nb 3QMAS spectra of the PMN/PSN solid solutions. We are now able to simulate 3QMAS spectra based on these NMR parameters and to use these to extract relative populations for each configuration. For instance, in the simple case of PMN, the parameters of all seven nBn configurations $(N_{Mg}, 0, 6\text{-}N_{Mg})$ have been estimated (see Fig. 3 for quadrupole products and Eq. (9) for isotropic chemical shifts) and they are used to simulate the two-dimensional spectrum using program DMFIT [18]; this is presented in Fig. 8.

In addition to the intensities, the line broadening in both isotropic and MAS dimensions were allowed to vary. Since the large number of parameters involved in fitting such a two-dimensional spectrum put high demands on the efficiency and robustness on the program, the fit shown in Fig. 8 is not well-optimized. The fractional intensities for configurations $(N_{Mg}, 0, 6\text{-}N_{Mg})$ with $N_{Mg} = 0, 1, \ldots, 6$ are, respectively, 17, 4, 5, 24, 10, 31, and 8%, respectively. The narrow peak 6 ($N_{Mg} = 6$) is not well fit using single P_Q and δ_{iso}^{CS} values, since it actually consists of narrow distributions of both NMR parameters. This peak should have slightly higher intensity than 8%; in the previous MAS study, this peak has intensity 14.8% [10]. Although these partial intensities may have systematic errors, an interesting comparison can be made to the values 25.1, 1.2, 6.2, 16.5, 24.7, 19.8, and 6.6% for $(N_{Mg}, 0, 6\text{-}N_{Mg})$ with $N_{Mg} = 0, 1, \ldots, 6$, respectively, which are predicted by random B-site model (see Table 2 of the previous MAS work) [10].

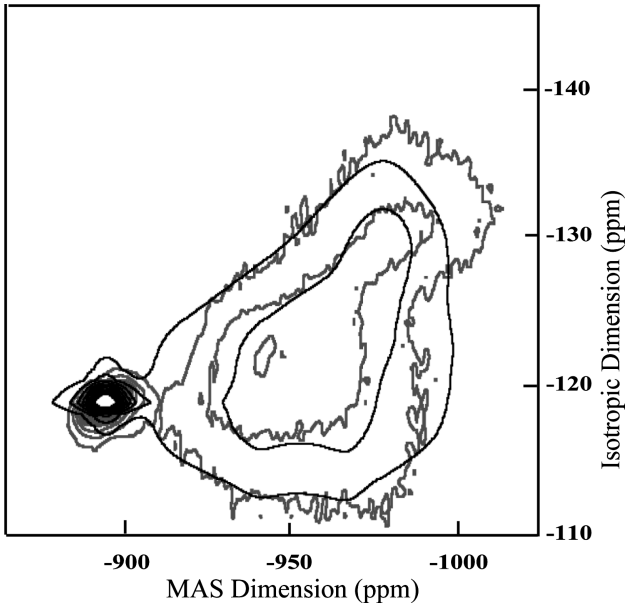

Fig. 8. Comparison of experimental (grey) and simulated (black) 3QMAS spectra of PMN using the NMR parameters calculated for the seven nBn configurations $(N_{Mg}, 0, 6\text{-}N_{Mg})$ with $N_{Mg} = 0, 1, \ldots, 6$. See Fig. 3 for quadrupole products and Eq. (9) for isotropic chemical shifts.

For higher PSN concentrations, there are more contributing configurations and it is not possible to extract the P_Q values of every configuration from the data. All these factors further complicate the modeling of two-dimensional spectra. Moreover for sites with different quadrupole coupling products, the excitation and transfer efficiencies in a MQMAS experiment are not as uniform as in a MAS experiment. A more efficient, tractable algorithm for obtaining more accurate partial intensities is to deconvolve a MAS spectrum using the δ_{iso}^{CS} values obtained by analyzing a MQMAS spectrum. In the previous study, we have already obtained reliable partial intensities for the narrow peaks by deconvoluting ^{93}Nb MAS spectra for the PMN/PSN solid-solutions [10]. Using these intensities we have been able to rule out the completely random B-site model, and support a modified random site model [10].

5. Conclusions

High-resolution ^{93}Nb 3QMAS experiments have been performed at high magnetic field strength (19.6 T) as a function of concentration in perovskite relaxor ferroelectric $(1-x)$PMN/xPSN solid-solutions. The higher resolution achievable in the two-dimensional experiment, together with the systematic investigation of concentration dependence, provides abundant structural information in these materials. We have been able to make clear and consistent assignments of spectral intensities to the 28 nearest B-site neighbor (nBn) configurations, (N_{Mg}, N_{Sc}, N_{Nb}), where each number ranges from 0 to 6 but their sum is constrained to 6. The seven narrow peaks are assigned to configurations of ^{93}Nb nuclei with only Mg^{2+} and/or Sc^{3+} cations occupying the six nearest B neighbor sites. The two broad components are assigned to configurations with more than one Nb^{5+} cation in the nearest B sites. Moreover, systematic analyses of the $(1-x)$PMN/xPSN 3QMAS spectra have enabled these Nb^{5+} containing configurations to be isolated and identified. NMR parameters have been calculated for most of the 28 possible nBn configurations. An empirical linear relationship has

been established between the observed isotropic chemical shift and the number of Mg^{2+} cations in the configuration; $\delta_{iso}^{CS} = (13.7 \pm 0.1)N_{Mg} - 970 \pm 0.4$ ppm. Enhanced 3QMAS resolution permits, for the first time, the quadrupole coupling product P_Q values to be determined for most of the 28 possible nBn configurations. The seven Nb^{5+}-deficient configurations (N_{Mg}, 6-N_{Mg}, 0) with $N_{Mg} = 0, 1, \ldots, 6$ and the pure niobium configuration (0, 0, 6) have small P_Q in the range 6–12 MHz. These have the smallest EFG due to the highly symmetric environment of the central niobium, implying that structural displacements and distortions must be small or dynamically averaged. The configurations with mixed Mg^{2+} and Nb^{5+}, or with mixed Sc^{3+} and Nb^{5+}, or with all three types of B-cations, have large quadrupole products $P_Q = 19$–40 MHz. It is interesting to notice that the five Mg, one Nb configuration configuration (5, 0, 1) has much larger P_Q (40 MHz) than that of the one Mg, five Nb configuration (1, 0, 5) (19 MHz). None are close to the value of 63 MHz reported in another NMR study [25].

With these values of NMR parameters, the relative displacement of ions in the solid solutions may be ultimately calculated from ab initio computational modeling. To understand ^{93}Nb chemical shift in perovskites, especially the intriguing observation that the 6-niobium and 6-scandium configurations have similar δ_{iso}^{CS} values, ab initio calculations need to be carried out using density function theory (DFT) and the gauge-including atomic orbital (GIAO) method, which have been used for calculating chemical shifts of ^{1}H, ^{13}C, ^{87}Rb, etc. [26–29]. To better understand the effects of nBn configurations on P_Q ab initio calculations of the electric field gradient should be carried out using either the MO LCAO-SCF (molecular orbitals-linear combinations of atomic orbitals-self-consistent field) or LDA LAPW (local density approximation using extended general potential linearized augmented plane wave method) approach. The former approach has been successfully applied to calculate the EFGs at the transition-metal sites in $LiNbO_3$ and $LiTaO_3$ crystals and at the aluminum sites in mixed ionic crystals $CaRAlO_4$ (R = La, Pr, Eu, Y) [30,31]; the latter approach has been applied to calculate the EFGs at the cation sites in $BaTiO_3$ and KNO_3 [32,33].

In conclusion, the current 3QMAS study has confirmed and refined the assignment of spectral components to nearest B-site neighbor configurations, which was first proposed in our MAS NMR study [10]. Moreover, the superb fidelity and accuracy of 3QMAS allows unprecedented detailed structural information and distribution of local disorder in complex materials. Thus, MAS and 3QMAS NMR techniques combined can be used to quantitatively study local structures and B-site cation ordering, which are very important for the relaxor ferroelectric properties of these materials.

Acknowledgments

Dr. P.K. Davies (University of Pennsylvania) is thanked for providing the well characterized PMN/PSN samples. Dr. Z. Gan (NHMFL, Tallahassee, Florida) is thanked for assistance in acquiring the 19.6 T 3QMAS spectra. We are grateful to Dr. F. Fayon and Dr. D. Massiot (CNRS, France) for helpful discussions. The National Science Foundation (Grant CHE 0079136) and the College of William and Mary are acknowledged for financial support.

References

[1] R.E. Newnham, Tunable transducers: nonlinear phenomena in electroceramics, NIST Spec. Publ. 804 (1996) 39–52.
[2] K. Uchino, Piezoelectric Actuators and Ultrasonic Motors, Kluwer Academic Publishers, Boston, 1996.
[3] S.-E. Park, T.R. Shrout, Ultrahigh strain and piezoelectric behavior in relaxor based ferroelectric single crystals, J. Appl. Phys. 82 (4) (1997) 1804–1811.
[4] L.E. Cross, Relaxor ferroelectrics: an overview, Ferroelectrics 151 (1994) 305–320.
[5] T. Egami, Microscopic model of relaxor phenomena in Pb containing mixed oxides, Ferroelectrics 222 (1999) 163–170.
[6] W. Dmowski, M.K. Akbas, P.K. Davies, T. Egami, Local structure of $Pb(Sc_{1/2},Ta_{1/2})O_3$ and related compounds, J. Phys. Chem. Solids 61 (2000) 229–237.
[7] L.E. Cross, Relaxor ferroelectrics, Ferroelectrics 76 (3–4) (1987) 241–267.
[8] M.A. Akbas, P.K. Davies, Domain growth in $Pb(Mg_{1/3},Ta_{2/3})O_3$ perovskite relaxor ferroelectric oxides, J. Am. Ceram. Soc. 80 (11) (1997) 2933–2936.
[9] J. Chen, H.M. Chan, M.P. Harmer, Ordering structure and dielectric properties of updoped and La/Na-doped $Pb(Mg_{1/3}, Nb_{2/3})O_3$, J. Am. Ceram. Soc. 72 (1989) 593–598.
[10] G.L. Hoatson, D.H. Zhou, F. Fayon, D. Massiot, R.L. Vold, ^{93}Nb MAS NMR study of perovskite relaxor ferroelectrics PMN-PSN, Phys. Rev. B 66 (2002) 224103.
[11] L. Frydman, J.S. Harwood, Isotropic spectra of half-integer quadrupolar spins from bidimensional magic-angle-spinning NMR, J. Am. Chem. Soc. 117 (1995) 5367–5368.
[12] A. Medek, J.S. Harwood, L. Frydman, Multiple-quantum magic-angle spinning NMR: a new method for the study of quadrupolar nuclei in solids, J. Am. Chem. Soc. 117 (1995) 12779–12787.
[13] P.K. Davies, L. Farber, M. Valant, M.A. Akbas, Cation ordering and dielectric properties of PMN-PSN relaxors, AIP Conf. Proc. 535 (2000) 38–46.
[14] J.-P. Amoureux, C. Fernandez, S. Steuernagel, Z filtering in MQMAS NMR, J. Magn. Reson., Ser. A 123 (1996) 116–118.
[15] F. Delaglio, G.W. Vuister, G. Zhu, J. Pfeifer, NMRPIPE: a multidimensional spectral processing system based on UNIX pipes, J. Biomol. NMR 6 (1995) 277–293.
[16] D. Massiot, B. Touzo, D. Trumeau, J.P. Coutures, J. Virlet, et al., Two-dimensional magic-angle spinning isotropic reconstruction sequences for quadrupolar nuclei, Solid State NMR 6 (1996) 73–83.
[17] P.R. Bodart, Distributions of the quadrupolar and isotropic chemical shift interactions in two-dimensional multiple-quantum MAS NMR spectra, J. Magn. Reson. 133 (1998) 207–209.
[18] D. Massiot, F. Fayon, M. Capron, I. King, S. Le Calve, B. Alonso, J.-O. Durand, B. Bujoli, Z. Gan, G. Hoatson, Modelling

one- and two-dimensional solid-state NMR spectra, Magn. Res. Chem. 40 (2002) 70–76.

[19] R.D. Shannon, Revised effective ionic radii and systematic studies of interatomic distances in halides and chalcogenides, Acta Cryst. A 32 (1976) 751–767.

[20] A.M. James, M.P. Lord, Macmillan's Chemical and Physical Data, Macmillan, London, UK, 1992.

[21] L.P. Cruz, J. Rocha, J.D.P. de Jesus, J.M. Savariault, J. Galy, Solid-state single and triple-quantum ^{93}Nb MAS NMR studies of ferroelectric $Pb(Mg_{1/3}Nb_{2/3})O_3$ and a related pyrochlore, Solid State NMR 15 (1999) 153–158.

[22] Y.-S. Kye, B. Herreos, G.S. Harbison, ^{207}Pb NMR and Monte Carlo studies of ionic solid solutions, Mat. Res. Soc. Symp. Proc. 547 (1999) 339–344.

[23] P. Bonneau, P. Garnier, G. Calvarin, E. Husson, J.R. Gavarri, A.W. Hewat, A. Morell, X-ray and neutron diffraction studies of the diffuse phase transition in PMN ceramics, J. Solid State Chem. 91 (1991) 350–361.

[24] I.-W. Chen, P. Li, Y. Wang, Structural origin of relaxor perovskites, J. Phys. Chem. Solids 57 (10) (1996) 1525–1536.

[25] S. Prasad, P. Zhao, J. Huang, J.S. Shore, Pure-phase two-dimensional niobium-93 nutation spectroscopic study of lead metaniobate and the piezoelectric lead magnesium niobate, Solid State NMR 14 (1999) 231–235.

[26] S.K. Wolff, T. Ziegler, E.V. Lenthe, E.J. Baerends, Density functional calculations of nuclear magnetic shieldings using the zeroth-order regular approximation (ZORA) for relativistic effects: ZORA nuclear magnetic resonance, J. Chem. Phys. 110 (16) (1999) 7689–7698.

[27] S.K. Wolff, T. Ziegler, Calculation of DFT-GIAO NMR shifts with the inclusion of spin-orbit coupling, J. Chem. Phys. 109 (3) (1998) 895–905.

[28] D.H. Kim, H.M. Eun, H.-S. Choi, Density functional theory/GIAO/CSGT studies of the ^{13}C NMR chemical shifts in 1-chlorosilatrane, Bull. Korean Chem. Soc. 21 (1) (2000) 148–150.

[29] A.C. de Dios, A. Walling, I. Cameron, C.I. Ratcliffe, J.A. Ripmeester, Alkali metal NMR chemical shielding as a probe of local structure: an experimental and theoretical study of Rb^+ in halide lattices, J. Phys. Chem. A 104 (2000) 908–914.

[30] M.G. Shelyapina, V.S. Kasperovich, B.F. Shchegolev, E.V. Charnaya, Ab initio cluster calculations of electric-field-gradients at the transition-metal sites in the ferroelectric $LiNbO_3$ and $LiTaO_3$ crystals, in: Proceedings of the 15th European Experimental NMR Conference (EENC), 2000.

[31] L.S. Vorotilova, O.E. Kvyatkovski, A.A. Levin, B.F. Shchegolev, Nonempirical cluster calculations of the electric field gradient tensor at the ^{27}Al nuclei in $YAlO_3$ and $HoAlO_3$ and refinement of the crystal structure of $HoAlO_3$, Phys. Solid State 35 (2) (1993) 143–145.

[32] T.J. Bastow, H.J. Whitfield, ^{137}Ba and ^{47,49}Ti NMR: electric field gradients in the non-cubic phases of $BaTiO_3$, Solid State Commun. 117 (2001) 483–488.

[33] D.J. Singh, Electric field gradients in $BaTiO_3$ and $KNbO_3$, Ferroelectrics 153 (1994) 183–187.